

# Magnetic Helicity Generation by Solar Differential Rotation

C. Richard DeVore

Laboratory for Computational Physics and Fluid Dynamics, Naval Research Laboratory,  
Washington, DC, 20375-5344; devore@nrl.navy.mil

Received \_\_\_\_\_; accepted \_\_\_\_\_

## ABSTRACT

Observations of sunspots, active regions, filaments, coronal arcades, and interplanetary magnetic clouds indicate that the Sun preferentially exhibits left-handed, negative-helicity features in its northern hemisphere, and their opposite counterparts in the south, independent of sunspot cycle. We investigate quantitatively the generation of magnetic helicity by solar differential rotation acting on emerged bipolar sources of flux, using analytical and numerical methods. We find that the vast majority of bipoles absorb negative helicity in the northern hemisphere and positive helicity in the south, in accord with observations. After two to four solar rotation periods have elapsed, the helicity generated by differential rotation amounts to about 10% of the bipole’s squared flux. Thus, each of the approximately  $1 \times 10^3$  large bipolar regions emergent on the Sun during sunspot cycle 21 entrained about  $1 \times 10^{43}$  Mx<sup>2</sup> of helicity in its  $1 \times 10^{22}$  Mx of flux. We show further that the roughly  $5 \times 10^3$  coronal mass ejections and associated interplanetary magnetic clouds that departed the Sun during the cycle carried off about  $5 \times 10^{24}$  Mx of flux and  $1 \times 10^{46}$  Mx<sup>2</sup> of helicity, within a factor of two of the estimates for solar production of these quantities. Evidently, differential rotation acting on emerged bipolar sources of flux can account quantitatively for the magnetic helicity balance of the Sun and the heliosphere, as well as for the observed prevalence of negative-helicity magnetic features in the north and positive-helicity features in the south.

*Subject headings:* Sun: activity — Sun: magnetic fields — solar wind

## 1. INTRODUCTION

Over the past decade, it has become increasingly clear that several global patterns of chirality, or handedness, are manifested in the Sun’s magnetic fields and their associated plasma structures (Rust 1994; Zirker et al. 1997; Martin 1998). A quantitative, mathematical measure of the chiral properties of these structures is the *magnetic helicity* (Moffatt 1978; Berger & Field 1984; Brown, Canfield, & Pevtsov 1999). The observed patterns exhibit helicities that are opposed in the northern and southern hemispheres, but are independent of sunspot cycle, i.e., of the sign of the Sun’s global dipole field. Features exhibiting such patterns include sunspot whorls, active region fields, eruptive X-ray loops, filaments and their accompanying fibrils and coronal arcades, and interplanetary magnetic clouds.

The earliest reports of chiral magnetic patterns on the Sun (Hale 1927; Richardson 1941) showed that some 80% of sunspots with discernible whorls showed a clockwise rotation of the fibril pattern in the southern hemisphere and a counter-clockwise rotation in the north. Similar patterns among the fields of solar active regions were found by Seehafer (1990), who compiled force-free field reconstructions from line-of-sight magnetograms showing that fields of positive helicity were dominant in the south and negative in the north. Positive helicity implies a right-handed twist and a clockwise rotation of flux when viewed from above, so his results agreed with those of Hale and Richardson. More recent work using vector magnetograms (Pevtsov, Canfield, & Metcalf 1995) confirmed that the helicity rule was obeyed in about 70% of cases studied. Similar percentages of the transient X-ray loop brightenings associated with coronal mass ejections (Webb 1992) display S-shaped, right-handed structures in the southern hemisphere, and their mirror images in the north (Rust & Kumar 1996; Canfield, Hudson, & McKenzie 1999).

Analyses of  $H\alpha$  images and photospheric magnetograms have revealed two analogous

chiralities of filaments, dextral and sinistral (Martin, Bilimoria, & Tracadas 1994), which prevail in the northern and southern solar hemispheres, respectively. Subsequent studies of the coronal X-ray arcades overlying filaments (Martin & McAllister 1997) have shown that left-handed arcades invariably are associated with dextral filaments, and right-handed with sinistral. These patterns are fully consistent with those for the fields of sunspots, active regions, and X-ray loops. Moreover, Rust & Martin (1994) found a one-to-one relationship between counterclockwise whorls and dextral filaments, and between clockwise whorls and sinistral filaments, in sunspots with both discernible whorls and adjacent filaments. This strongly suggests that dextral filaments contain left-handed, negative-helicity fields (Rust & Kumar 1994; Rust 1999), consistent with the flow patterns reported for a number of quiescent prominences (Gigolashvili 1978), although some (e.g., Martin 1998) dissent from this view.

Interplanetary magnetic clouds (Burlaga et al. 1981; Goldstein 1984; Burlaga 1988; Lepping, Jones, & Burlaga 1990) also are threaded by substantially twisted, helical fields, and have been linked very strongly to *disparition brusques*, or disappearing filaments, on the Sun (Marubashi 1986; Wilson & Hildner 1986). It has been established that these clouds exhibit the same chirality as their underlying solar phenomena (Rust 1994; Bothmer & Schwenn 1994, 1998; Bothmer & Rust 1997). Evidently, the disappearing filaments erupt into the corona and then traverse the heliosphere within the solar wind, conveying their imbedded magnetic flux and helicity along with them.

Exceptions to these helicity patterns occur in most categories of solar activity. Nevertheless, the Sun's preference for features adhering to these rules over such a broad range of scales motivates the search for an underlying mechanism that is, evidently, global in scope. Two principal candidates have been proposed (e.g., Seehafer 1990): the twisting of magnetic fluxtubes in the convection zone, where dynamo action amplifies the fields prior to

their appearance at the surface; and the shearing of the magnetic fields after emergence, by the large-scale flows of the Sun’s differential rotation. Evidence for the dynamo mechanism, in which the helicity is already contained in twisted fluxtubes when they erupt, includes the cited observations of chirality patterns in relatively young, developed active regions (Seehafer 1990; Pevtsov et al. 1995) and more recent observations of strong electric currents and helicity generation in newly emerging magnetic flux (Leka et al. 1996; Wang 1996). All of these results suggest strongly that the solar dynamo makes an important contribution to the Sun’s helicity budget.

However, the solar differential rotation can make a substantial, possibly dominant, contribution, as well. Many of the bipolar regions appearing on the Sun are very large in scale and persist for several rotations (cf. Sheeley 1992), allowing the relatively slow rotational shear to build up considerable twist in the field. As noted first by Sturrock & Woodbury (1967), this shear generates negative helicity in the northern hemisphere and positive helicity in the south. More recently, van Ballegooijen (1999) simulated the combined effects of differential rotation and supergranular diffusion on bipolar magnetic loops. He found that negative helicity is generated in bipoles in the north, whether initially untwisted or containing a finite amount of initial helicity, thereby creating new or enhancing initially left-handed fields and unwinding initially right-handed fields.

Our principal objective in this paper is to quantify the generation of helicity in bipolar regions by the Sun’s nonuniform rotation, for comparison with observations. Most determinations of the ‘helicity’ in solar active regions are restricted specifically to the current helicity, whose volumetric density is  $\mathbf{B} \cdot \nabla \times \mathbf{B}$  and which is a measure of the topological properties, such as twist and mutual linkages, of the lines of electric current (Moffatt 1978; Berger & Field 1984). Much preferred, however, is the magnetic helicity, whose density is  $\mathbf{A} \cdot \nabla \times \mathbf{A} = \mathbf{A} \cdot \mathbf{B}$  and which reflects the topology of the magnetic field.

Although the need to compute the vector potential  $\mathbf{A}$  makes the evaluation of the magnetic helicity more difficult, it is the superior measure because it reflects the properties of the magnetic field directly. In addition, it is perfectly conserved while convected with the flow in ideal magnetohydrodynamics (MHD) (Moffatt 1978), and is thought to be a rugged invariant in highly conducting laboratory (Taylor 1986) and space (Berger 1999) plasmas such as the solar corona.

As a model problem, we adopt the initial potential field generated by a dipole embedded below a plane surface, and subject it to a linear shear flow on that surface. The initial helicity generation rate is calculated analytically, and the asymptotic behavior is determined through numerical simulation. Using observational data for solar bipolar regions, we then estimate the total magnetic helicity produced during their individual lifetimes and over an entire sunspot cycle. Similarly, we use a model and data for interplanetary magnetic clouds to estimate their entrained magnetic flux and helicity. These two quantities for the Sun and the solar wind agree with each other to within a factor of two. We also find good agreement between the force-free field parameters derived from our simulations and those measured in solar active regions. Our results strongly support the conjectures that differential rotation, acting on emerged magnetic flux, makes a substantial contribution to the Sun’s magnetic-helicity balance and may play an essential role in producing the observed chiral patterns of magnetic activity.

## 2. SHEARED BIPOLAR MAGNETIC REGIONS

### 2.1. Theory

The magnetic helicity is defined by the volume integral

$$H_M = \int dV \mathbf{A} \cdot \mathbf{B}, \tag{1}$$

where  $\mathbf{A}$  is the vector potential,

$$\mathbf{B} = \nabla \times \mathbf{A}, \quad (2)$$

and the integral is evaluated over the entire coronal volume. In general, the helicity is gauge-invariant, and thereby unique, only when the surfaces bounding the coronal volume are magnetic surfaces (i.e.,  $\hat{\mathbf{n}} \cdot \mathbf{B}|_S = 0$  is satisfied everywhere). For the corona, bounded below by the photosphere, this condition is not met. A gauge-invariant helicity still can be obtained, however, by subtracting off the helicity of a corresponding current-free field which has the same distribution of vertical magnetic flux at the photospheric bounding surface (Berger & Field 1984). If the vector potential  $\mathbf{A}_c$  for that field satisfies the Coulomb gauge ( $\nabla \cdot \mathbf{A}_c = 0$ ) and has a vanishing normal component at the base ( $\hat{\mathbf{n}} \cdot \mathbf{A}_c|_S = 0$ ), then the potential helicity integral vanishes and we are left with the expression (1) for  $H_M$ .

A suitable  $\mathbf{A}_c$  can be constructed straightforwardly from the corresponding scalar potential,  $\phi_c$ , for the current-free field. The scalar potential, in turn, can be evaluated as an integral over the base plane, using Green's function for Laplace's equation as the integration kernel. In cartesian geometry  $(x, y, z)$ , where  $z$  is the height above the bounding coronal surface, we have

$$\phi_c(x, y, z, t) = \frac{1}{2\pi} \int \int dx' dy' \frac{B_z(x', y', 0, t)}{[(x - x')^2 + (y - y')^2 + z^2]^{1/2}}. \quad (3)$$

Now, we set

$$\mathbf{A}_c(x, y, z, t) = \nabla \times \hat{\mathbf{z}} \int_z^\infty dz' \phi_c(x, y, z', t). \quad (4)$$

From this definition and  $\nabla^2 \phi_c = 0$  it follows readily that

$$\nabla \times \mathbf{A}_c = -\nabla \phi_c, \quad (5)$$

i.e., the magnetic fields produced by these scalar and vector potentials are identical.

The results for  $\mathbf{A}_c$  at the coronal base,  $z = 0$ , are used to set the boundary values for

the vector potential  $\mathbf{A}$  for the actual magnetic field  $\mathbf{B}$ . An integration yields

$$\mathbf{A}(x, y, z, t) = \mathbf{A}_c(x, y, 0, t) - \hat{\mathbf{z}} \times \int_0^z dz' \mathbf{B}(x, y, z', t). \quad (6)$$

The volume helicity integral  $H_M$  now can be evaluated directly.

Alternatively, the rate of helicity generation can be computed from a surface integral over the base. In ideal MHD, the result for the production rate is (e.g., Berger & Field 1984)

$$\frac{dH_M}{dt} = -2 \int \int dx dy [(\mathbf{A}_c \cdot \mathbf{v}) \mathbf{B} - (\mathbf{A}_c \cdot \mathbf{B}) \mathbf{v}] \cdot \hat{\mathbf{z}}. \quad (7)$$

The first term on the right side describes the generation of helicity by horizontal motions of the footpoints, while the second term represents the emergence or submergence of pre-existing helicity by flows through the base plane. We consider only the footpoint-generation mechanism in this paper. The numerical calculations to be described later use both the volume helicity integral and the surface rate integral as diagnostics. To study the problem analytically, we employ the surface rate integral, as follows.

As a model for the initial field of bipolar regions at the photosphere and above, we assume a horizontal point dipole, with a characteristic (signed) field amplitude  $B_0$ , embedded a depth  $d$  below the surface  $z = 0$ . The  $x$  direction of the cartesian coordinate system is aligned with solar longitude, i.e., with the direction of the differential rotation's shear flow, and the  $y$  direction with solar latitude. The tilt angle  $\chi$  of the region is defined with respect to the lines of longitude. It is positive if the dipole axis is rotated clockwise with respect to the vertical, and negative otherwise. Northern-hemisphere bipolar regions then usually have positive tilt angles, while those in the south generally have negative tilt angles.

The resulting scalar potential for the initial field is

$$\phi_c(x, y, z, 0) = B_0 d^3 \frac{x \cos \chi - y \sin \chi}{[x^2 + y^2 + (z + d)^2]^{3/2}}. \quad (8)$$

Evaluating the  $z$  integral of this function yields the vector potential,

$$\mathbf{A}_c(x, y, z, 0) = \nabla \times \hat{\mathbf{z}} B_0 d^3 \frac{x \cos \chi - y \sin \chi}{x^2 + y^2} \left( 1 - \frac{z + d}{[x^2 + y^2 + (z + d)^2]^{1/2}} \right), \quad (9)$$

while its negative  $z$  derivative gives the vertical field,

$$B_z(x, y, z, 0) = 3B_0 d^3 (z + d) \frac{x \cos \chi - y \sin \chi}{[x^2 + y^2 + (z + d)^2]^{5/2}}. \quad (10)$$

For the shear velocity associated with the differential rotation, we use the local, linear form

$$\mathbf{v} = \Omega y \hat{\mathbf{x}}. \quad (11)$$

On the Sun, the shear coefficient  $\Omega$  is negative in the north and positive in the south.

These expressions, evaluated at  $z = 0$ , are substituted into the surface integral for the helicity generation rate. In this case, the integral reduces to

$$\frac{dH_M}{dt} = -2 \int \int dx dy A_{cx} v_x B_z. \quad (12)$$

Several of the resulting terms vanish due to symmetry. The remainder can be simplified and combined by converting the integration variables to cylindrical polar coordinates.

Evaluating the resulting integrals yields for the initial rate of helicity generation

$$\left. \frac{dH_M^{bmr}}{dt} \right|_{t=0} = \frac{\pi}{8} \Omega B_0^2 d^4 \cos 2\chi. \quad (13)$$

Since the magnitude of the flux of either polarity threading the base plane is

$$\Phi = 2|B_0|d^2, \quad (14)$$

as can be established from the expression for  $B_z$ , the generation rate can be rewritten as

$$\left. \frac{dH_M^{bmr}}{dt} \right|_{t=0} = \frac{\pi}{32} \Omega \Phi^2 \cos 2\chi. \quad (15)$$

Thus, our analysis predicts an initial rate of helicity generation that is about 10% of the product of the local shear coefficient, the square of the magnetic flux in the region, and the cosine of twice the bipole's tilt angle with respect to lines of longitude.

Before considering the implications of this result for the Sun, we first address the later evolution of the helicity generation process. As time passes, the vertical field  $B_z$  and vector potential  $A_{cx}$  evolve away from the initial values assumed above. The derived expression for  $dH_M/dt$  then no longer applies. It is possible, but cumbersome, to compute small departures from the initial rate by expressing  $B_z$  as a Taylor series in  $\Omega t$  and solving the resulting induction equation to derive the spatial dependence. The resulting first-order correction to equation (15), for example, is proportional to  $\Omega^2 t \Phi^2 \sin 2\chi$ . To study the time-asymptotic development of the bipolar region and determine the total helicity generated over its lifetime, however, requires solving the problem with its full, nonlinear time dependence. For this, we must turn to numerical techniques.

## 2.2. Simulations

To simulate numerically the late-time development of the sheared, bipolar magnetic field, we used our new, time-dependent, magnetohydrodynamics model *FCTMHD3D*. It is a three-dimensional (3D) extension of our previous MHD models, and employs similar flux-corrected transport (*FCT*) techniques ( DeVore 1991) to advance the equations in time. *FCTMHD3D* was implemented on massively parallel computers to permit its use in lengthy, slowly evolving simulations on well-resolved grids.

Our model solves the time-dependent, ideal MHD equations appropriate for the solar corona:

$$\frac{\partial \rho}{\partial t} + \nabla \cdot (\rho \mathbf{v}) = 0, \tag{16}$$

$$\frac{\partial \rho \mathbf{v}}{\partial t} + \nabla \cdot (\rho \mathbf{v} \mathbf{v}) = -\nabla P + \frac{1}{4\pi} (\nabla \times \mathbf{B}) \times \mathbf{B}, \tag{17}$$

$$\frac{\partial U}{\partial t} + \nabla \cdot (U \mathbf{v}) = -P \nabla \cdot \mathbf{v}, \tag{18}$$

$$\frac{\partial \mathbf{B}}{\partial t} = \nabla \times (\mathbf{v} \times \mathbf{B}), \tag{19}$$

where  $\rho$  is the mass density,  $\mathbf{v}$  is the velocity,  $P$  is the gas pressure,  $\mathbf{B}$  is the magnetic field, and  $U$  is the internal energy density,  $U = P/(\gamma - 1) = 3P/2$ .

For all but the very largest bipolar regions, the effect of the curvature of the solar surface is negligible, so we use a cartesian coordinate system, as we did in our analytical treatment above. The equations can be made dimensionless by scaling out a mass density  $\rho_0$ , field strength  $B_0$ , and region size  $L$ , and appropriate combinations of those parameters for other quantities such as velocity ( $B_0/\rho_0^{1/2}$ ) and magnetic helicity ( $B_0^2 L^4$ ). This freedom can be used to arbitrarily set the uniform mass density, the characteristic length, and the magnetic flux of each polarity in the initial numerical state, for convenience. Results for realistic solar parameters can be recovered by applying the appropriate scaling factors.

Open boundary conditions, with zero-gradient extrapolations of all variables, were used on the four sides and the top of the domain. At the base plane, we held the mass density  $\rho$  and pressure  $P$  fixed at their initial values, set the horizontal velocities to those of the differential rotation, i.e.,  $v_x = \Omega y, v_y = 0$ , and required the vertical velocity to vanish,  $v_z = 0$ . The magnetic field at the base was extrapolated assuming zero gradient, as was done at the remaining five boundaries.

We carried out two lengthy sequences of simulation runs, both initialized with bipoles of depth  $d = L = 2$  and strength  $B_0 = 8$ . The initial mass density  $\rho_0 = 1$  and plasma pressure  $P_0 = 0.01$  were uniform in our model corona, and the resultant plasma  $\beta = 8\pi P/B^2$  ranged upwards from  $4 \times 10^{-3}$ . We set the shear coefficient to  $\Omega = -5 \times 10^{-3} B_0/\rho_0^{1/2} L = -2 \times 10^{-2}$ . The sign is appropriate for the Sun’s northern hemisphere, and the magnitude corresponds to a velocity shear across the bipole of about 2% ( $5\sqrt{4\pi} \times 10^{-3}$ ) of the peak Alfvén speed. This guaranteed a slow, quasi-static evolution of the coronal field in response to the imposed footpoint motions. Although those motions were at least an order of magnitude faster than the corresponding differential rotation velocities on the Sun, they served the critical

purpose of consuming less than 10% of the computation time needed to obtain solutions otherwise. We would not expect to see any significant differences between our results and others obtained for more realistic velocities, save for the change in time scales.

The computational domain extended over  $[-10, +10]$  in  $x$  and  $y$ , and over  $[0, 10]$  in  $z$ . The nonuniform grid was stretched exponentially away from the origin, in all three directions, from roughly cubic cells of size  $2.6 \times 10^{-2}$ . The spacing was stretched by a factor of 14 along  $x$  and  $y$  and by a factor of 8 along  $z$ . About one-third of the grid points lay within  $[-1, +1]$  along  $x$  and  $y$ , and nearly one-half within  $[0, 2]$  along  $z$ . The full grid for these simulations was  $150 \times 150 \times 120$ .

Our two cases were selected to bracket the extremes of tilt angle  $\chi$ , suggested by the analytical treatment of the previous section. The initial helicity generation rate, equation (15), is proportional to  $\cos 2\chi$ . To confirm this prediction and explore the later time development of the helicity, we examined the cases  $\chi = 0$  (no tilt; a horizontal bipole) and  $\chi = \pi/2$  (maximum tilt; a vertical bipole). Only the first case is typically observed on the Sun, at least among the relatively large bipolar regions of importance to the solar magnetic-helicity balance. Those regions are known to exhibit a finite, systematic tilt which increases with latitude - i.e., they obey Joy's law (Hale et al. 1919) - but the tilt angles are relatively small. This topic is discussed further below, with reference to observational data.

The resultant helicity generation rates  $dH_M/dt$  and magnetic helicities  $H_M$  are illustrated in Figures 1 and 2, for the horizontal and vertical bipoles, respectively. Both the rates and helicities are normalized, the rates to  $(\pi/32)|\Omega|\Phi^2$  and the helicities to  $(\pi/32)\Phi^2$ , and displayed as functions of the normalized time  $|\Omega|t$ . The initial rates agree very well with the predicted values,  $-\cos 2\chi = \mp 1$ , for the respective cases. The slopes of these curves, i.e., the second time derivatives  $d^2H_m/dt^2$ , are zero initially. This too is consistent with our linearized analysis, whose first correction to the initial generation rate is proportional

to  $\sin 2\chi$ . These contributions vanish for our two bipoles. As time passes, the helicity generation rates gradually decline in magnitude and eventually weakly change sign, at about time  $t \sim 2/|\Omega|$ . The extremal total helicities reached for the horizontal and vertical bipoles were  $-0.93$  and  $+0.77$ , respectively. Following the sign reversal of the generation rates, the helicities retreated slowly and modestly from these values.

Our numerical results suggest that, within factors of order unity, we can describe the generation of magnetic helicity in solar bipolar regions by differential rotation as follows. The initial generation rate is given by the analytical result in equation (15),

$$\left. \frac{dH_M^{bmr}}{dt} \right|_{t=0} \sim \frac{\pi}{32} \Omega \Phi^2 \cos 2\chi. \quad (20)$$

Over a characteristic helicity generation time  $\tau^{bmr}$ , given by

$$\tau^{bmr} \sim 2/|\Omega|, \quad (21)$$

the generation rate falls to essentially zero. At that time, the total magnetic helicity that has been generated is approximately

$$\begin{aligned} H_M^{bmr} &\sim \frac{1}{2} \tau^{bmr} \left. \frac{dH_M^{bmr}}{dt} \right|_{t=0} \\ &\sim \text{sgn}(\Omega) \frac{\pi}{32} \Phi^2 \cos 2\chi, \end{aligned} \quad (22)$$

where the sign function is

$$\begin{aligned} &= -1, \quad x < 0, \\ \text{sgn}(x) &= 0, \quad x = 0, \\ &= +1, \quad x > 0. \end{aligned} \quad (23)$$

Thus, the total magnetic helicity generated is about 10% of the product of the squared flux in the bipole, the cosine of twice its tilt angle, and the sign of the shear coefficient in the hemisphere hosting the flux.

For further comparison with observations, we have computed the volume-averaged, force-free parameter  $\alpha$  for our simulated bipoles. A quasistatic, strong magnetic field in the low-pressure corona must be force-free, with the electric current aligned with the magnetic field, viz.,

$$\nabla \times \mathbf{B} = \alpha \mathbf{B}. \quad (24)$$

An average value of  $\alpha$  for the region can be calculated from

$$\langle \alpha \rangle = \frac{\int dV \alpha B^2}{\int dV B^2} = \frac{\int dV \mathbf{B} \cdot \nabla \times \mathbf{B}}{\int dV \mathbf{B} \cdot \mathbf{B}}. \quad (25)$$

The results, normalized to the inverse length  $L^{-1}$ , are shown in Figure 3. For the horizontal bipole,  $\langle \alpha \rangle$  rises monotonically throughout, reaching a value of about -2 when the magnetic helicity peaks near time  $\tau^{bmr}$ . In contrast,  $\langle \alpha \rangle$  for the vertical bipole plateaus at a value of about +1/2 at time  $\tau^{bmr}/2$ , and very gradually declines thereafter. The signs would be reversed for a region in the southern hemisphere. Only the result for the horizontal bipole is generally relevant to the Sun, for which we therefore can take

$$\langle \alpha \rangle^{bmr} \sim \text{sgn}(\Omega) \frac{2}{L}. \quad (26)$$

### 2.3. Application to the Sun

To apply these theoretical and numerical results to the Sun requires data for the properties of the bipolar regions appearing on it. A record of the strengths, polarities, and locations of the leading and following fluxes of the bipoles emergent during sunspot cycle 21 (1976-1986) was derived from Kitt Peak National Observatory magnetograms by N. R. Sheeley, Jr. (Sheeley, DeVore, & Boris 1985; Wang & Sheeley 1989). This source list has been used extensively by Sheeley and collaborators in a number of studies of the large-scale solar magnetic field during sunspot cycle 21 (Sheeley 1992, and references therein).

In their statistical analysis of the source record for cycle 21, Wang & Sheeley divided the bipoles into three groups - strong, medium, and weak - with the divisions between them set arbitrarily at  $5 \times 10^{21}$  Mx and  $2 \times 10^{21}$  Mx of flux. The strong group comprised about 25% of the bipoles measured (710 of 2710) and contained about 65% of the total flux ( $7 \times 10^{24}$  Mx of  $11 \times 10^{24}$  Mx). The average strength of a source in the strong group was  $1 \times 10^{22}$  Mx. In addition, the greatest contribution to the total flux that emerged during cycle 21 came from bipoles with fluxes of that amount. Thus, we use

$$\Phi^{bmr} \sim 1 \times 10^{22} \text{ Mx} \quad (27)$$

as a nominal measure of the flux contained in large solar bipolar regions.

Wang & Sheeley also measured and displayed the tilt angles of the bipoles in their three flux groups, and in the sample as a whole, as a function of the centroidal latitude of the bipoles. The plot is very nearly linear, rising from about  $2.5^\circ$  of tilt at  $5^\circ$  latitude to about  $15^\circ$  of tilt at  $30^\circ$  latitude. The tilt was defined to be positive if the leading flux was equatorward of the following flux. In our coordinate system, this would be a clockwise (positive) rotation away from lines of longitude in the north, and counterclockwise (negative) in the south. Consequently, the Wang-Sheeley measured tilt angle  $\chi$  satisfies

$$\chi \approx \psi/2, \quad (28)$$

where  $\psi$  is the signed latitude of the bipole's center of flux, positive in the north and negative in the south. This is a quantitative expression of Joy's law (Hale et al. 1919).

A simple form for the Sun's latitude-dependent rate of rotation is

$$\omega(\psi) = \omega_0 - \omega_2 \sin^2 \psi, \quad (29)$$

where  $\omega_0, \omega_2 > 0$ , so that the equator rotates more rapidly than the poles. Larger bipolar regions occasionally host long-lived sunspots, and are long-lived themselves, so for their

rotation rate we use the value measured by Newton & Nunn (1951),

$$\omega_2 = 2.77 \text{ deg day}^{-1} = 4.83 \times 10^{-2} \text{ rad day}^{-1}. \quad (30)$$

We difference the rotation rate  $\omega(\psi)$  over a latitude increment  $\Delta\psi$  and multiply by the distance  $R_\odot \cos \psi$  of the region from the Sun's axis of rotation. The resultant shear velocity is

$$\begin{aligned} v(\psi) &= R_\odot \cos \psi \frac{\partial \omega}{\partial \psi} \Delta\psi, \\ &= -2\omega_2 \cos^2 \psi \sin \psi R_\odot \Delta\psi, \end{aligned} \quad (31)$$

whence

$$\Omega(\psi) = -2\omega_2 \cos^2 \psi \sin \psi \quad (32)$$

is the required shear coefficient, since  $\Delta y = R_\odot \Delta\psi$ .

Combining these results for the tilt angle (28) and the shear coefficient (32), we find that the initial helicity generation rate (15) takes the form

$$\left. \frac{dH_M^{bmr}}{dt} \right|_{t=0} = -\frac{\pi}{32} \Phi^2 2\omega_2 \cos^3 \psi \sin \psi. \quad (33)$$

This expression is negative in the northern solar hemisphere and positive in the south. As a function of latitude, it attains its peak magnitude at  $\psi = \pm 30^\circ$ . For our nominal bipole with  $1 \times 10^{22}$  Mx of flux and the Newton-Nunn rate of differential rotation, the generation rate there is

$$\left. \frac{dH_M^{bmr}}{dt} \right|_{t=0} \sim -\text{sgn}(\psi) 3 \times 10^{41} \text{ Mx}^2 \text{ day}^{-1}. \quad (34)$$

The resultant total helicity produced, from equation (22), is

$$H_M^{bmr} \sim -\text{sgn}(\psi) \frac{\pi}{32} \Phi^2 \cos \psi, \quad (35)$$

or

$$H_M^{bmr} \sim -\text{sgn}(\psi) 1 \times 10^{43} \text{ Mx}^2 \quad (36)$$

for our nominal bipole.

The corresponding helicity generation time (21) is

$$\tau^{bmr} \sim 2/|\Omega| = 1/|\omega_2| |\cos^2 \psi \sin \psi|, \quad (37)$$

whence

$$\begin{aligned} \tau^{bmr} &\sim 54 \text{ days } (\psi = 35^\circ), \\ &\sim 108 \text{ days } (\psi = 11^\circ). \end{aligned} \quad (38)$$

The smaller, higher-latitude value for  $\tau^{bmr}$  is the minimum over the entire Sun. The larger value obtains near the peak of the profile of total flux emerged during cycle 21 versus latitude, as found by Wang & Sheeley. These generation times correspond to approximately two and four solar rotation periods, respectively. Four rotation periods also is roughly the lifetime of the Sun’s large bipolar regions, after which their flux becomes dispersed among and merges with the large-scale background fields (e.g., Sheeley 1992). At still lower latitudes, the differential rotation rate is slow enough that the flux of the bipoles is dispersed before it can be fully charged with helicity. This modification produces a rapid but smooth change in the profile of helicity generation across the Sun’s equator, rather than the discontinuity suggested by our idealized expression (22). Elucidating the details of this transition would require additional simulations including the effects of diffusion on the bipolar fields, and is beyond the scope of the present paper.

Wang & Sheeley also displayed the pole separation as a function of source strength for their bipolar regions. A bipole with  $1 \times 10^{22}$  Mx of flux has an average pole separation of about  $8^\circ$ , whence

$$L \sim 8 \frac{\pi}{180} R_\odot \sim 1 \times 10^{10} \text{ cm}. \quad (39)$$

The associated force-free parameter  $\alpha$  (26) at the end of the helicity-generation process is,

for a bipole with modest tilt,

$$\langle \alpha \rangle^{bmr} \sim -\text{sgn}(\psi) 2 \times 10^{-10} \text{ cm}^{-1}, \quad (40)$$

comparable to the values measured in solar active regions (Seehafer 1990; Pevtsov et al. 1995; Leka et al. 1996; Wang 1996).

Finally, we noted above that more than 700 bipoles of nominal strength  $1 \times 10^{22}$  Mx erupted on the Sun during cycle 21. Thus, the total emergent flux and the total magnetic helicity generated by differential rotation over the cycle are

$$\Phi^{Sun} \sim 1 \times 10^3 \Phi^{bmr} \sim 1 \times 10^{25} \text{ Mx} \quad (41)$$

and

$$|H_M^{Sun}| \sim 1 \times 10^3 |H_M^{bmr}| \sim 1 \times 10^{46} \text{ Mx}^2, \quad (42)$$

respectively. In §3.2 we compare these estimates with corresponding estimates for interplanetary magnetic clouds.

### 3. INTERPLANETARY MAGNETIC CLOUDS

#### 3.1. Theory

Burlaga et al. (1981) described interplanetary magnetic clouds as structures of the order of an AU in size, possessing a high average field strength, a low average plasma pressure, and a magnetic field direction that rotates monotonically through a large angle as the cloud transits the solar system. Goldstein (1984) first proposed that interplanetary magnetic clouds could be modeled as cylindrically symmetric fluxtubes with force-free magnetic fields. Burlaga (1988) later suggested simplifying the model by assuming that the electric current was a constant, uniform multiple of the magnetic field. He used the

resulting model to fit several cases of observed magnetic clouds by trial and error. A more systematic approach to the fitting procedure, employing least-squares techniques, was developed by Lepping et al. (1990) and applied to a sample of 18 observed clouds.

Burlaga’s model is based on Lundquist’s (1950) constant- $\alpha$ , force-free magnetic field,

$$\begin{aligned} B_r &= 0, \\ B_\phi &= \sigma_H B_0 J_1 \left( \alpha_0 \frac{r}{r_0} \right), \\ B_z &= B_0 J_0 \left( \alpha_0 \frac{r}{r_0} \right), \end{aligned} \tag{43}$$

where  $B_0$  is the signed, axial field of the flux rope,  $\sigma_H = \pm 1$  selects a right- or left-handed helical field near the axis, respectively,  $r_0$  measures the radial extent of the structure,  $J_n$  is the Bessel function of the first kind of order  $n$ , and  $\alpha_0$  is a dimensionless parameter fixed by the boundary conditions. Differentiation of this field yields the constant- $\alpha$ , force-free condition

$$\nabla \times \mathbf{B} = \sigma_H \frac{\alpha_0}{r_0} \mathbf{B} \equiv \alpha \mathbf{B} \tag{44}$$

To fit the cloud data, the Lundquist solution is truncated at radius  $r_0$  and matched to a potential field at larger radii. In particular, to yield a single reversal of the azimuthal field of the flux rope during passage, the outer boundary is placed at the first zero of the Bessel function  $J_0$ , where the axial field vanishes. This condition fixes  $\alpha_0$  (Abramowitz & Stegun 1964):

$$J_0(\alpha_0) = 0, \quad \alpha_0 = 2.40. \tag{45}$$

As illustrated by Burlaga and Lepping et al., the resulting field changes from purely axial at  $r = 0$  to purely azimuthal at  $r = r_0$ , producing a smooth,  $180^\circ$  rotation of the field direction as the flux rope passes the observer.

Rearranging (44) for the constant- $\alpha$  force-free field yields the vector potential

$$\mathbf{A} = \frac{1}{\alpha} \mathbf{B} = \sigma_H \frac{r_0}{\alpha_0} \mathbf{B}. \tag{46}$$

Gauge-invariance of the magnetic helicity is automatically ensured for the flux rope, since the boundary  $r = r_0$  is a flux surface ( $\mathbf{B} \cdot \hat{\mathbf{n}} = B_r = 0$  there), and the volume outside contributes nothing since the field is potential beyond  $r = r_0$ . Assuming a length  $\ell$  for the cylindrical flux rope, then, the helicity of the interplanetary magnetic cloud,  $H_M^{imc}$ , is

$$\begin{aligned} H_M^{imc} &= 2\pi\ell\sigma_H\frac{r_0}{\alpha_0}\int_0^{r_0} dr r B^2 \\ &= \sigma_H B_0^2 r_0^3 \ell \frac{2\pi}{\alpha_0} \int_0^1 dx x \left[ J_0^2(\alpha_0 x) + J_1^2(\alpha_0 x) \right]. \end{aligned} \quad (47)$$

Evaluating the integrals analytically (Gradshteyn & Ryzhik 1965) and then numerically (Abramowitz & Stegun 1964) yields the dimensionless coefficient

$$\frac{\pi}{\alpha_0} \left[ J_1^2(\alpha_0) + J_2^2(\alpha_0) \right] = 0.60, \quad (48)$$

whence

$$H_M^{imc} = 0.60\sigma_H B_0^2 r_0^3 \ell. \quad (49)$$

Similarly, the axial flux contained in the cloud can be computed from

$$\begin{aligned} \Phi^{imc} &= \left| 2\pi \int_0^{r_0} dr r B_z \right| \\ &= |B_0| r_0^2 2\pi \int_0^1 dx x J_0(\alpha_0 x). \end{aligned} \quad (50)$$

The dimensionless coefficient is

$$\frac{2\pi}{\alpha_0} J_1(\alpha_0) = 1.4, \quad (51)$$

whence

$$\Phi^{imc} = 1.4 |B_0| r_0^2. \quad (52)$$

### 3.2. Application to the Heliosphere

In their study of interplanetary clouds and the fitting of Lundquist's force-free cylindrical solution to the observed fields, Lepping et al. determined and tabulated the

parameters of 18 well-observed clouds. An average over their dataset gave

$$\begin{aligned} |B_0| &= 2 \times 10^{-4} \text{ G}, \\ r_0 &= 2 \times 10^{12} \text{ cm}. \end{aligned} \tag{53}$$

About half of the clouds observed contained right-handed, or positive-helicity, fields. To estimate the length  $\ell$  of the flux rope, we use the fact that several of the clouds extended at least  $30^\circ$  in longitude at 1 AU. Hence, we take

$$\ell \sim \frac{\pi}{6} \text{ AU} \sim 1 \times 10^{13} \text{ cm}. \tag{54}$$

This estimate also is consistent with the average measured angular extent ( $\sim 40^\circ$ ) of coronal mass ejections during sunspot cycle 21 (Webb & Howard 1994). Upon substitution into equation (49) we obtain for the helicity of a typical interplanetary magnetic cloud

$$H_M^{imc} \sim \sigma_H 2 \times 10^{42} \text{ Mx}^2. \tag{55}$$

The corresponding magnetic flux contained in the cloud is, from (52),

$$\Phi^{imc} \sim 1 \times 10^{21} \text{ Mx}. \tag{56}$$

To estimate the number of interplanetary magnetic clouds transiting the heliosphere over the duration of the sunspot cycle, we use the results of Webb & Howard (1994). They reported an occurrence rate for coronal mass ejections during cycle 21 corresponding to more than 4000 events, and an even larger number of disappearing filaments and eruptive limb prominences combined. Let us assume that the small sample of clouds studied in detail by Lepping et al. (1990) is representative of all clouds. Then, over an entire cycle, we expect the solar wind to transport a total flux and helicity in clouds associated with solar eruptive events of

$$\Phi^{Wind} \sim 5 \times 10^3 \Phi^{imc} \sim 5 \times 10^{24} \text{ Mx}. \tag{57}$$

and

$$|H_M^{Wind}| \sim 5 \times 10^3 |H_M^{imc}| \sim 1 \times 10^{46} \text{ Mx}^2, \quad (58)$$

respectively. These estimates agree, to within a factor of two, with those obtained earlier for the flux and helicity appearing in bipolar regions on the Sun, (41) and (42). Also, since the volume  $V_{Wind}$  of a spherical shell of plasma passing the earth at  $500 \text{ km s}^{-1}$  over the 11-year cycle is about  $5 \times 10^{43} \text{ cm}^3$ , we find for the average helicity density in interplanetary clouds in the solar wind at 1 AU

$$|h_M^{Wind}| = |H_M^{Wind}|/V_{Wind} \sim 200 \text{ Mx}^2 \text{ cm}^{-3}. \quad (59)$$

This estimate is in excellent agreement with direct measurements of the average net helicity density associated with coronal mass ejections during cycles 20-22, with an additional, roughly equal amount contributed by the Parker spiral in the background solar wind (Smith 1999).

#### 4. SUMMARY AND DISCUSSION

The principal results of our study relate the rate and time scale of magnetic helicity generation, the total helicity produced, and the resultant force-free parameter for a solar bipolar region to its initial flux, tilt angle, and pole separation, and the local shear coefficient associated with differential rotation. We evaluated these expressions for a nominal bipolar region appearing on the Sun with  $1 \times 10^{22} \text{ Mx}$  of flux, a pole separation of  $10^{10} \text{ cm}$ , and a tilt angle of about half the latitude (Wang & Sheeley 1989). We found that about  $1 \times 10^{43} \text{ Mx}^2$  of magnetic helicity are produced in such a region over its lifetime, yielding an average force-free parameter  $\alpha$  of about  $2 \times 10^{-10} \text{ cm}^{-1}$ . The latitude-dependent generation rate is as high as  $3 \times 10^{41} \text{ Mx}^2 \text{ day}^{-1}$ , peaking at about  $30^\circ$  latitude. All of these quantities have the same sign and are nearly always negative in the northern solar hemisphere, and positive

in the south. The helicity generation ebbs and then weakly reverses after 50 to 100 days, or two to four solar rotation periods, have passed. Accumulated over the roughly  $1 \times 10^3$  such regions which emerge during the sunspot cycle, we find that the Sun processes about  $1 \times 10^{25}$  Mx of large-scale magnetic flux through its surface per cycle, which differential rotation winds up to generate about  $1 \times 10^{46}$  Mx<sup>2</sup> of magnetic helicity in the corona.

In order to avoid a monotonic accumulation of flux and helicity in its atmosphere as time passes, the Sun must submerge an equal amount of these quantities back into its interior or shed them into the solar wind. The mechanism for the latter is the coronal mass ejection associated with a disappearing filament or eruptive X-ray loop, which is manifested as an interplanetary magnetic cloud propagating outwards along with the solar wind (Marubashi 1986; Wilson & Hildner 1986; Webb 1992; Rust 1994; Bothmer & Schwenn 1994, 1998; Bothmer & Rust 1997). We found that a typical cloud (Lepping et al. 1990) contains about  $1 \times 10^{21}$  Mx of flux and  $2 \times 10^{42}$  Mx<sup>2</sup> of helicity. Accumulated over the approximately  $5 \times 10^3$  such events occurring over the sunspot cycle (Webb & Howard 1994), we find that about  $5 \times 10^{24}$  Mx of flux and  $1 \times 10^{46}$  Mx<sup>2</sup> of helicity are ejected by the Sun in the form of magnetic clouds. The latter also is fully consistent with an average helicity density in ejecta of  $200 \text{ Mx}^2 \text{ cm}^{-3}$  at 1 AU, convected at the  $500 \text{ km s}^{-1}$  speed of the solar wind (Smith 1999). These estimates for the total flux and helicity in clouds are within a factor of two of our corresponding numbers for solar production of these quantities.

In contrast, Bieber & Rust (1995) and Rust (1997) estimated that the Sun would shed significantly smaller amounts,  $1 \times 10^{24}$  Mx and  $2 \times 10^{45}$  Mx<sup>2</sup>, respectively, of magnetic flux and helicity over the sunspot cycle. They based their estimate on a model of subsurface winding of the Sun’s poloidal field by differential rotation. This produces toroidal flux that erupts to form active regions, and eventually escapes the surface to be carried off with the solar wind. The effect of differential rotation on emerged flux was ignored. Their

multiparameter model can be adjusted readily in several ways to accommodate a higher rate of helicity generation and shedding, which clearly is needed to conform with the observations. Our model, unlike theirs, matches the total magnetic flux shed and helicity generated by the Sun with no adjustable parameters.

We did use several idealizations and estimates in our analysis and simulations that affect the accuracy of our quantitative results, to within probably a factor of two at most. These include the use of an idealized potential field as the initial state for our bipolar regions; the approximations of a linear shear profile and a cartesian geometry; and the parameters assumed for our nominal solar bipolar region. We neglected the influence of turbulent diffusion of flux on the evolution of the bipoles (van Ballegoijen 1999), but this too is unlikely to have a substantial effect on our results for large, long-lived regions. The opposite is true for small, short-lived bipoles, but they make a negligibly small contribution to the Sun’s total helicity in any case. The mutual helicity of neighboring, interacting bipoles (Berger 1999) may be important occasionally, particularly in complexes of activity featuring recurring eruptions of new flux. Again, however, only modest changes in our quantitative results are expected, in the absence of very tangled structures containing multiple linkages between bipoles.

Thus, our results strongly suggest that the shearing of bipolar regions by differential rotation contributes substantially, if not predominantly, to the Sun’s total magnetic helicity. We found that  $1 \times 10^{43}$  Mx<sup>2</sup> of helicity will be generated over the lifetime of a region with  $1 \times 10^{22}$  Mx of flux. To our knowledge, the only quantitative estimate of the helicity in an observed solar active region was made by Wang (1996), who deduced that  $\sim 1 \times 10^{43}$  Mx<sup>2</sup> of helicity was produced in an emerging-flux region over a period of just a few hours. The corresponding generation rate was  $1 \times 10^{44}$  Mx day<sup>-1</sup>, three orders of magnitude faster than our rate due to differential rotation. This example demonstrates clearly the

importance of helicity emergence in at least some solar active regions. However, a much more widely used measure of the helicity in emerging and developed active regions is the force-free parameter  $\alpha$ . We obtained a volume-averaged value of  $2 \times 10^{-10} \text{ cm}^{-1}$  for our nominal bipolar region, which is within a factor of three of observational estimates for this parameter (Seehafer 1990; Pevtsov et al. 1995; Leka et al. 1996; Wang 1996). As a proxy for the magnetic helicity present in newly emerging and young active regions, the observed force-free parameters suggest that the solar dynamo produces about as much helicity prior to emergence as does differential rotation after emergence. Quantifying the relative importance of these contributions to the Sun’s total magnetic helicity requires further research, especially measures of the amounts of helicity emerging in the form of new flux and residing in mature, fully developed active regions.

We did not consider any net helicity to be present in our initial bipoles. This could be adjusted easily in additional numerical experiments by first twisting the flux in the loops, moving the footpoints along contours of constant vertical field (van Ballegooijen 1999). Such motions would generate helicity in the overlying coronal flux without modifying the vertical field or the current-free vector potential at the photosphere. Thereafter applying the differential rotation to the resulting, twisted loop would generate additional helicity at the same rate as for our untwisted, current-free loop; the helicity-generation integral would be unchanged. Thus, any pre-existing net helicity produced by the envisioned twisting would simply change the zero point of the helicity for our new case. This initial helicity would be augmented or depleted with time, according to its sign and that of the rate of generation by differential rotation.

Our results further suggest that differential rotation acting on the Sun’s emerged sources of magnetic flux nearly invariably creates left-handed, negative-helicity fields in the northern hemisphere, and their right-handed, positive-helicity counterparts in the south.

This is consistent with the chiral patterns observed in sunspot whorls, active region fields, eruptive X-ray loops, filaments and their fibrils and arcades, and interplanetary magnetic clouds. The rule for differential rotation is not inviolate, due to the dependence of the resultant helicity on the tilt angle of the bipole. Regions tilted more than  $45^\circ$  to the horizontal are twisted in the opposite sense to those tilted less than  $45^\circ$ . However, only about 5% of solar flux emerges at such high tilt angles (Wang & Sheeley 1989), and most of that at angles only slightly in excess of  $45^\circ$ , where the generation rate vanishes. Thus, differential rotation produces helicity in emerged bipolar flux in such a way as to obey the observed chirality rules essentially all of the time.

This leaves unexplained the not-infrequent exceptions to some of the observed patterns. About 20% of sunspot whorls (Hale 1927; Richardson 1941) and 30% of active regions (Pevtsov et al. 1995) and transient X-ray loop brightenings (Rust & Kumar 1996; Canfield et al. 1999) exhibit the minority helicity in the hemisphere in which they occur. These percentages are far higher than the 5% of exceptions anticipated for differential rotation acting on erupted bipolar flux. Thus, we conclude that helicity generation by surface differential rotation cannot account for those solar features with minority chirality.

On the other hand, it also has been asserted (e.g., van Ballegoijen & Martens 1990; Rust & Kumar 1994; Rust 1997) that the observed patterns of quiescent filaments cannot be understood based on the action of differential rotation on emerged solar flux. The argument is that a potential-field arcade whose polarity inversion line is oriented east-west will be sheared to generate helicity of the wrong sign. This conclusion is undeniably correct, and is supported by our analysis and simulations of a bipole tilted at  $90^\circ$ . However, we contend that the premise is wrong-headed: flux does not emerge on the Sun in the form of potential arcades with east-west inversion lines, but rather as bipolar regions with roughly north-south inversion lines. As time passes and differential rotation shears the flux of these

bipoles, the inversion lines rotate toward a more east-west orientation. Late in the regions' development, although the rate of helicity generation reverses sign, it thereafter remains small in magnitude. As our simulations for a horizontal bipole demonstrate, the helicity produced during the early life of the region has the correct sign and is only modestly reduced in magnitude during this late phase. It is these remnant fields, left-handed with negative helicity in the north, and their opposite counterparts in the south, that are available to participate in the formation of filaments and other chiral features in their respective hemispheres, in accordance with the observed patterns.

Finally, our results suggest an important constraint on models for solar eruptive behavior. We observed that comparable total amounts of magnetic flux and helicity are contained in the bipolar regions sheared by the Sun's nonuniform surface rotation and in the helically wound interplanetary clouds transiting the heliosphere, over the course of the sunspot cycle. This is in accord with expectations that these quantities should be at least approximately conserved in a highly conducting plasma such as the solar corona (Taylor 1986; Berger 1999). On the other hand, there are 5-10 times as many eruptive events as there are large active regions, with each remnant cloud containing only 10-20% of the flux and helicity of each original bipole. This clearly favors eruption mechanisms that at any one time allow only a small portion of the field comprising typical large-scale solar structures to escape. The remaining flux and helicity are left behind, evidently, to be reconfigured and eventually ejected in subsequent events. It is well known that many, if not all, solar eruptions originate in multipolar magnetic configurations (Hu et al. 1996; Webb et al. 1997; Innes et al. 1999), rather than in simple bipolar structures such as isolated loops. This complexity is fully compatible with our model of global conservation of magnetic flux and helicity and their shedding by the corona. It also is compatible with observations of interplanetary clouds as helically twisted, force-free, constant- $\alpha$  flux ropes: the latter are just the minimum-energy states of magnetic fields with prescribed helicity (Woltjer 1958),

in low-pressure plasmas such as the solar wind.

It is a pleasure to acknowledge the hospitality of Richard C. Canfield and Alexei A. Pevtsov and the High Altitude Observatory at NCAR, organizers and hosts of a stimulating Chapman conference on magnetic helicity in space and laboratory plasmas. The author is grateful for illuminating discussions regarding magnetic helicity generation with Adrian A. van Ballegoijen and the Sun's bipolar sources of flux with Neil R. Sheeley, Jr. Thanks also are due Jean E. Osburn for facilitating access to the supercomputing resources required for this study, and Judith T. Karpen for her helpful comments on a draft of the manuscript.

The development of *FCTMHD3D* was sponsored by NASA's High Performance Computing and Communications program in Earth and Space Sciences, and the numerical simulations were performed using grants of time from the DoD's High Performance Computing Modernization Program. Research support also was provided by NASA's program in Sun-Earth Connection Theory.

## REFERENCES

- Abramowitz, M., & Stegun, I. A. 1964, Handbook of Mathematical Functions (Washington: U.S. GPO)
- Berger, M. A. 1999, in Magnetic Helicity in Space and Laboratory Plasmas, ed. Brown, M. R., Canfield, R. C., & Pevtsov, A. A. (Washington: AGU), 1
- Berger, M. A., & Field, G. B. 1984, *J. Fluid Mech.*, 147, 133
- Bieber, J. W., & Rust, D. M. 1995, *ApJ*, 453, 911
- Bothmer, V., & Rust, D. M. 1997, in Coronal Mass Ejections, ed. Crooker, N., Joselyn, J. A., & Feynman, J. (Washington: AGU), 139
- Bothmer, V., & Schwenn, R. 1994, *Space Sci. Rev.*, 70, 215
- Bothmer, V., & Schwenn, R. 1998, *Ann. Geophys.*, 16, 1
- Brown, M. R., Canfield, R. C., & Pevtsov, A. A. 1999, *Magnetic Helicity in Space and Laboratory Plasmas* (Washington: AGU)
- Burlaga, L. F. 1988, *J. Geophys. Res.*, 93, 7217
- Burlaga, L. F., Sittler, E., Mariani, F., & Schwenn, R. 1981, *J. Geophys. Res.*, 86, 6673
- Canfield, R. C., Hudson, H. S., & McKenzie, D. E. 1999, *Geophys. Res. Lett.*, 26, 627
- DeVore, C. R. 1991, *J. Comp. Phys.*, 92, 142
- Gigolashvili, M. S. 1978, *Sol. Phys.*, 60, 293
- Goldstein, H. 1984, in *Solar Wind Five*, ed. Neugebauer, M. (Washington: NASA), 731

- Gradshteyn, I. S., & Ryzhik, I. M. 1965, *Table of Integrals, Series, and Products* (New York: Academic)
- Hale, G. E. 1927, *Nature*, 119, 708
- Hale, G. E., Ellerman, F., Nicholson, S., & Joy, A. 1919, *ApJ*, 49, 153
- Hu, F. M., Song, M. T., Liu, Q. Z., & Ji, H. S. 1996, *Sol. Phys.*, 165, 395
- Innes, D. E., Inhester, B., Srivastava, N., Brekke, P., Harrison, R. A., Matthews, S. A., J. C. Noens, Schmieder, B., & Thompson, B. J. 1999, *Sol. Phys.*, 186, 337
- Leka, K. D., Canfield, R. C., McClymont, A. N., & van Driel-Gesztelyi, L. 1996, *ApJ*, 462, 547
- Lepping, R. P., Jones, J. A., & Burlaga, L. F. 1990, *J. Geophys. Res.*, 95, 11957
- Lundquist, S. 1950, *Ark. Fys.*, 2, 361
- Martin, S. F. 1998, in *New Perspectives on Solar Prominences*, ed. Webb, D., Rust, D., & Schmieder, B. (San Francisco: ASP), 419
- Martin, S. F., Bilimoria, R., & Tracadas, P. W. 1994, in *Solar Surface Magnetism*, ed. Rutten, R. J., & Schrijver, C. J. (Dordrecht: Kluwer), 303
- Martin, S. F., & McAllister, A. H. 1997, in *Coronal Mass Ejections*, ed. Crooker, N., Joselyn, J. A., & Feynman, J. (Washington: AGU), 127
- Marubashi, K. 1986, *Adv. Space Res.*, 6, 335
- Moffatt, H. K. 1978, *Magnetic Field Generation in Electrically Conducting Fluids* (New York: Cambridge)
- Newton, H. W., & Nunn, M. L. 1951, *MNRAS*, 111, 413

- Pevtsov, A. A., Canfield, R. C., & Metcalf, T. R. 1995, *ApJ*, 440, L109
- Richardson, R. S. 1941, *ApJ*, 41, 24
- Rust, D. M. 1994, *Geophys. Res. Lett.*, 21, 241
- Rust, D. M. 1997, in *Coronal Mass Ejections*, ed. Crooker, N., Joselyn, J. A., & Feynman, J. (Washington: AGU), 119
- Rust, D. M. 1999, in *Magnetic Helicity in Space and Laboratory Plasmas*, ed. Brown, M. R., Canfield, R. C., & Pevtsov, A. A. (Washington: AGU), 221
- Rust, D. M., & Kumar, A. 1994, *Sol. Phys.*, 155, 69
- Rust, D. M., & Kumar, A. 1996, *ApJ*, 464, L199
- Rust, D. M., & Martin, S. F. 1994, in *Solar Active Region Evolution*, ed. Balasubramaniam, K. S., & Simon, G. W. (San Francisco: ASP), 337
- Seehafer, N. 1990, *Sol. Phys.*, 125, 219
- Sheeley, N. R., Jr. 1992, in *The Solar Cycle*, ed. Harvey, K. L. (San Francisco: ASP), 1
- Sheeley, N. R., Jr., DeVore, C. R., & Boris, J. P. 1985, *Sol. Phys.*, 98, 219
- Smith, C. W. 1999, in *Magnetic Helicity in Space and Laboratory Plasmas*, ed. Brown, M. R., Canfield, R. C., & Pevtsov, A. A. (Washington: AGU), 239
- Sturrock, P. A., & Woodbury, E. T. 1967, in *Proceedings of the International School of Physics ‘Enrico Fermi’*, ed. Sturrock, P. A. (New York: Academic), 155
- Taylor, J. B. 1986, *Rev. Mod. Phys.*, 58, 741
- van Ballegooijen, A. A. 1999, in *Magnetic Helicity in Space and Laboratory Plasmas*, ed. Brown, M. R., Canfield, R. C., & Pevtsov, A. A. (Washington: AGU), 213

- van Ballegooijen, A. A., & Martens, P. C. H. 1990, *ApJ*, 361, 2183
- Wang, J. 1996, *Sol. Phys.*, 163, 319
- Wang, Y.-M., & Sheeley, N. R., Jr. 1989, *Sol. Phys.*, 124, 81
- Webb, D. F. 1992, in *Eruptive Solar Flares*, ed. Svestka, Z., Jackson, B. V., & Machado, M. E. (New York: Springer), 234
- Webb, D. F., & Howard, R. A. 1994, *J. Geophys. Res.*, 99, 4201
- Webb, D. F., Kahler, S. W., McIntosh, P. S., & Klimchuk, J. A. 1997, *J. Geophys. Res.*, 102, 24161
- Wilson, R. M., & Hildner, E. 1986, *J. Geophys. Res.*, 91, 5867
- Woltjer, L. 1958, *Proc. Nat. Acad. Sci. USA*, 44, 489
- Zirker, J., Martin, S. F., Harvey, K., & Gaizauskas, V. 1997, *Sol. Phys.*, 175, 27

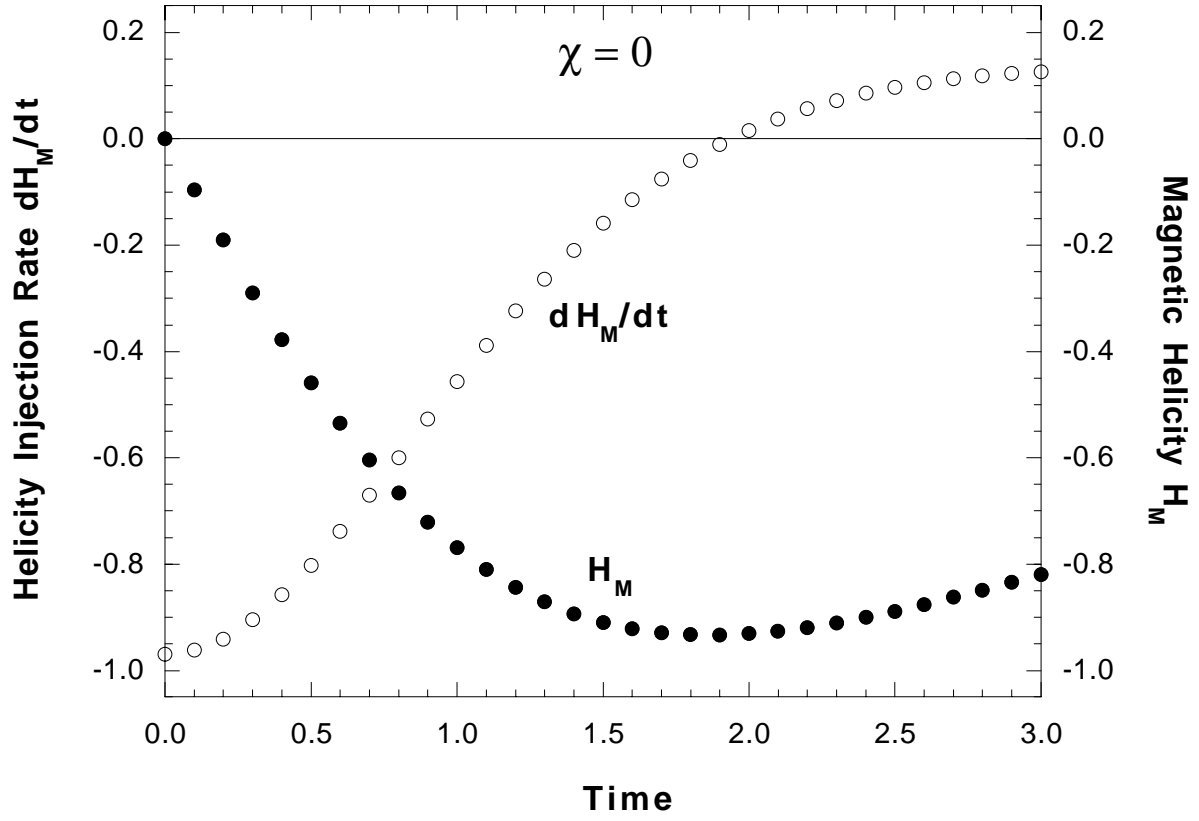


Fig. 1.— The normalized magnetic-helicity generation rate  $dH_M/dt$  (open circles) and accumulated magnetic helicity  $H_M$  (filled circles) displayed versus normalized time  $t$ , for a horizontal bipole (tilt angle  $\chi = 0$ ).

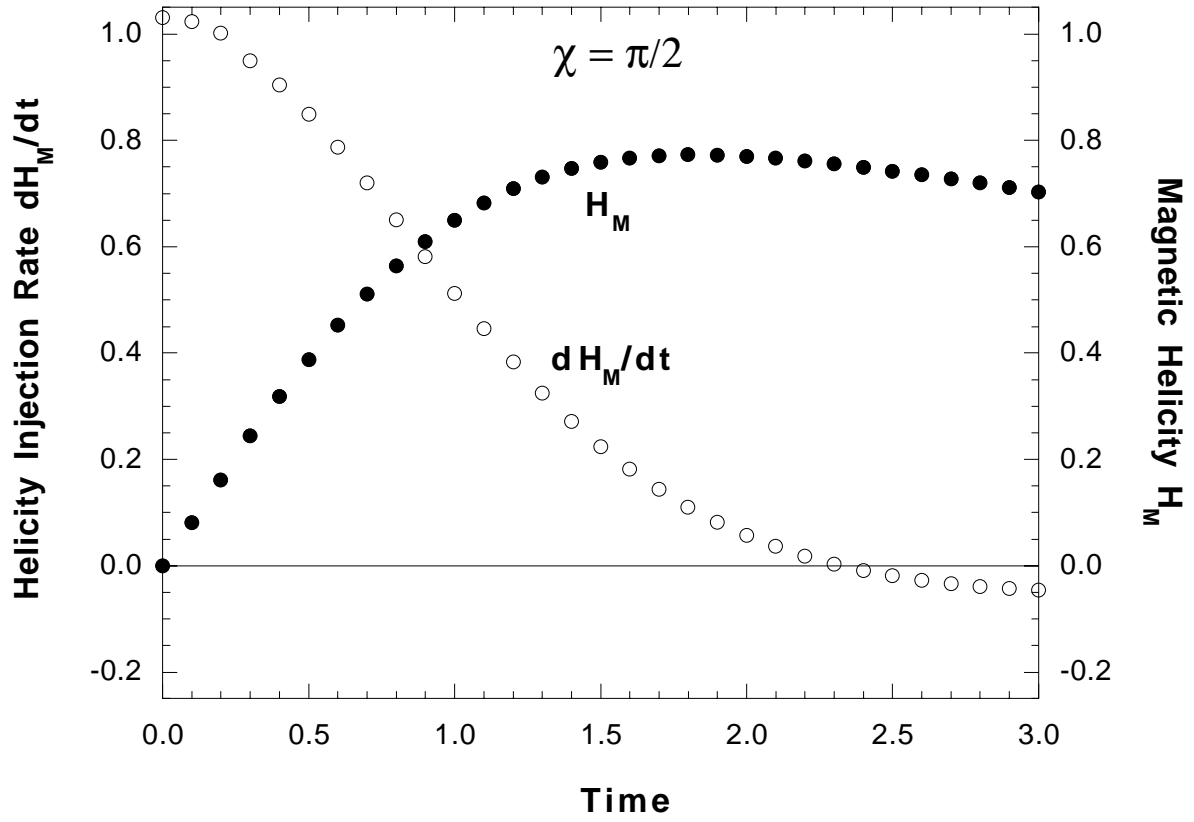


Fig. 2.— Same as Figure 1, for a vertical bipole (tilt angle  $\chi = \pi/2$ ).

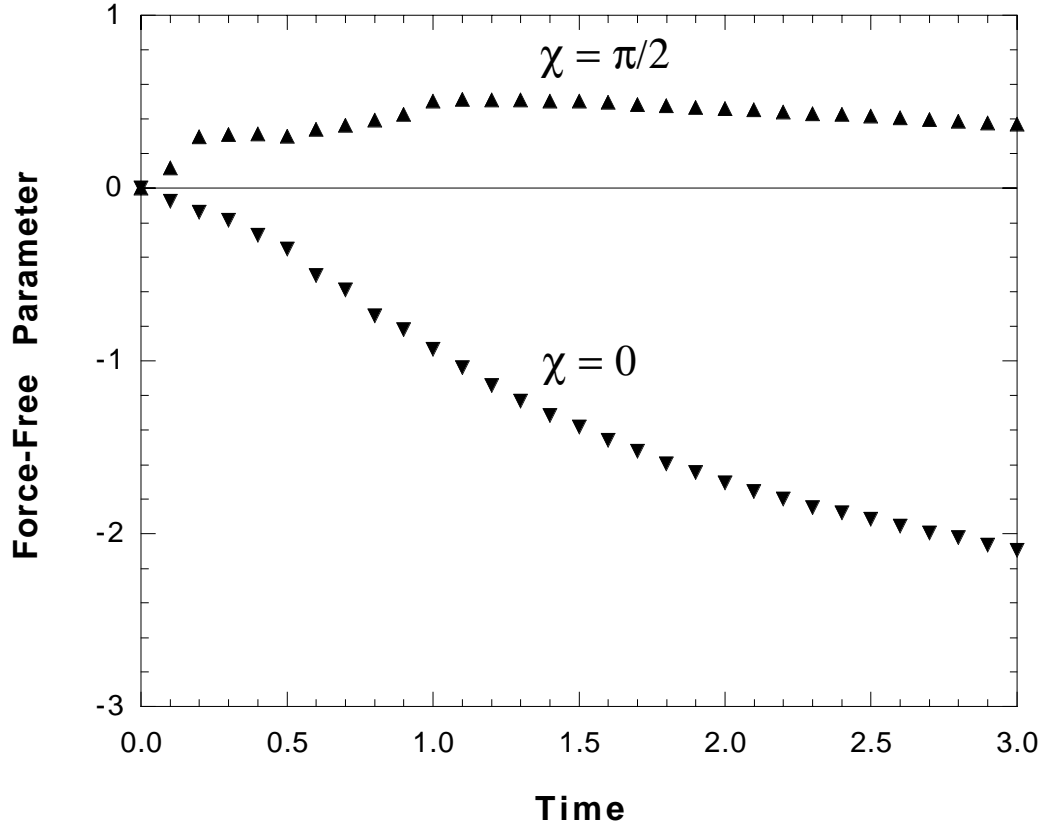


Fig. 3.— The normalized force-free parameter  $\alpha$ , displayed versus normalized time  $t$ , for the horizontal ( $\chi = 0$ ) and vertical ( $\chi = \pi/2$ ) bipoles in Figures 1 and 2, respectively.